









RESEARCH ARTICLE | MAY 24 2021

# Inverse spin-Hall effect in GeSn

A. Marchionni  ; C. Zucchetti   ; F. Ciccacci; M. Finazzi  ; H. S. Funk  ; D. Schwarz  ; M. Oehme  ; J. Schulze; F. Bottegoni 

 Check for updates

*Appl. Phys. Lett.* 118, 212402 (2021)

<https://doi.org/10.1063/5.0046129>



## Articles You May Be Interested In

Electric field modulation of spin transport

*APL Mater.* (January 2022)

Spin pumping and laser modulated inverse spin Hall effect in yttrium iron garnet/germanium heterojunctions

*Appl. Phys. Lett.* (March 2020)

Direct bandgap GeSn nanowires enabled with ultrahigh tension from harnessing intrinsic compressive strain

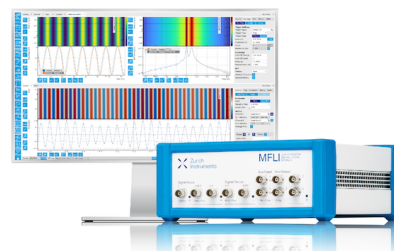
*Appl. Phys. Lett.* (May 2022)

# Challenge us.

What are your needs for periodic signal detection?



[Find out more](#)



# Inverse spin-Hall effect in GeSn

Cite as: Appl. Phys. Lett. **118**, 212402 (2021); doi: [10.1063/5.0046129](https://doi.org/10.1063/5.0046129)

Submitted: 1 February 2021 · Accepted: 19 April 2021 ·

Published Online: 24 May 2021



View Online



Export Citation



CrossMark

A. Marchionni,<sup>1</sup>  C. Zucchetti,<sup>1,a)</sup>  F. Ciccacci,<sup>1</sup> M. Finazzi,<sup>1</sup>  H. S. Funk,<sup>2</sup>  D. Schwarz,<sup>2</sup>  M. Oehme,<sup>2</sup>   
J. Schulze,<sup>2</sup> and F. Bottegoni<sup>1</sup> 

## AFFILIATIONS

<sup>1</sup>LNESS-Dipartimento di Fisica, Politecnico di Milano, Piazza Leonardo da Vinci 32, 20133 Milano, Italy

<sup>2</sup>Institute of Semiconductor Engineering (IHT), University of Stuttgart, Pfaffenwaldring 47, 70569 Stuttgart, Germany

<sup>a)</sup> Author to whom correspondence should be addressed: [carlo.zucchetti@polimi.it](mailto:carlo.zucchetti@polimi.it)

## ABSTRACT

Due to the long spin lifetime and its optical and electrical properties, GeSn is a promising candidate for the integration of spintronics, photonics, and electronics. Here, we investigate the photoinduced inverse spin-Hall effect in a GeSn alloy with 5% Sn concentration. We generate a spin-polarized electron population at the  $\Gamma$  point of the GeSn conduction band by means of optical orientation, and we detect the inverse spin-Hall effect signal coming from the spin-to-charge conversion in GeSn. We study the dependence of the inverse spin-Hall signal on the kinetic energy of the spin-polarized carriers by varying the energy of the impinging photons in the 0.5–1.5 eV range. We rationalize the experimental data within a diffusion model which explicitly accounts for momentum, energy, and spin relaxation of the spin-polarized hot electrons. At high photon energies, when the spin relaxation is mainly driven by phonon scattering, we extract a spin-Hall angle in GeSn which is more than ten times larger than the one of pure Ge. Moreover, the spin-charge interconversion for electrons lying at the  $\Delta$  valleys of GeSn results to be  $\approx 4.3$  times larger than the one for electrons at  $L$  valleys.

Published under an exclusive license by AIP Publishing. <https://doi.org/10.1063/5.0046129>

Group IV semiconductors are the materials of choice of modern electronics. The integration of spintronic features with the mainstream Si-based technology would thus be of extreme importance. A possible route is the study of magnon spintronics in ferromagnetic/semiconductor systems.<sup>1</sup> Alternatively, it is possible to directly study the spin-related properties of group-IV materials.<sup>2,3</sup> While spin-orbit phenomena are generally small in Si,<sup>4–6</sup> Ge displays relevant spin-related effects occurring in the bulk<sup>6–9</sup> or at the surface<sup>10</sup> and at interfaces with other materials.<sup>9,11,12</sup> The 4% lattice mismatch with Si allows for the implementation of Ge functionalities on the mainstream Si-based technology.<sup>13</sup> Moreover, typical spin-diffusion lengths in Ge are on the order of some micrometers,<sup>14–16</sup> and spin lifetime can be further enhanced in strain-engineered structures.<sup>17</sup>

In this context, Sn can be a convenient material for the development of a platform with increased spin-orbit coupling (SOC) within group-IV materials. The absence of an energy gap in Sn does not allow for field-effect operations. However, when less than 15% of Sn is diluted in Ge, the resulting alloy behaves as a semiconductor, with a gap larger than 0.4 eV.<sup>18,19</sup> Despite the small equilibrium solubility of Sn in Ge and the 14% lattice mismatch between the two materials,<sup>20,21</sup> high-quality GeSn alloys have been grown on Si.<sup>22</sup> This led, for instance, to the demonstration of the lasing action in GeSn.<sup>23</sup> Literature reports also suggest that the spin lifetime in GeSn lies in the

nanoseconds range,<sup>24</sup> making it an appealing material for the development of spin interconnects.<sup>25,26</sup> Conversely, other spintronics applications, e.g., ultrafast optical switches, require short spin lifetimes,<sup>27</sup> which can be reached by engineering the dopant concentration of GeSn. Hence, this alloy could represent a platform where optoelectronic and spintronic architectures can be conveniently implemented.<sup>28–30</sup>

In this work, we investigate the dependence of the spin-Hall angle, i.e., the efficiency of the spin-charge interconversion, as a function of the kinetic energy of the spin-polarized carriers of a Ge<sub>0.95</sub>Sn<sub>0.05</sub> alloy. We generate a spin population by means of optical orientation<sup>31–34</sup> at the  $\Gamma$  point of the GeSn conduction band, which undergoes spin-dependent scattering, generating an inverse spin-Hall effect (ISHE) electromotive field.<sup>35,36</sup> The optically injected spin current density  $\mathbf{j}_s$  is thus converted to a charge current density  $\mathbf{j}_c$ ,<sup>35,36</sup>

$$\mathbf{j}_c = \gamma \mathbf{j}_s \times \mathbf{u}_p, \quad (1)$$

$\gamma$  being the spin-Hall angle and  $\mathbf{u}_p$  the unit vector representing the direction of the spin-polarization. Experimentally, we detect the voltage drop  $\Delta V_{\text{ISHE}}$  across two electrodes at the edges of a GeSn bar, since  $\mathbf{j}_c$ <sup>12</sup> is a function of the incident photon energy, and characterize the spin transport properties of hot electrons.<sup>8</sup> From the measured signal and exploiting a model explicitly accounting for momentum, spin, and

energy relaxation of hot electrons, we infer the spin–charge interconversion efficiency  $\gamma$  as a function of the kinetic energy of the carriers. For incident photon energies much larger than the direct GeSn gap, the spin-dependent scattering is dominated by phonons, and we estimate  $\gamma \approx 0.3$ , a value ten times larger than the one of bulk Ge.<sup>8</sup> Moreover, in GeSn, we obtain a different efficiency of spin–charge interconversion for electrons diffusing at the  $L$  and  $\Delta$  valleys, the latter being a factor 4.3 larger than the former.

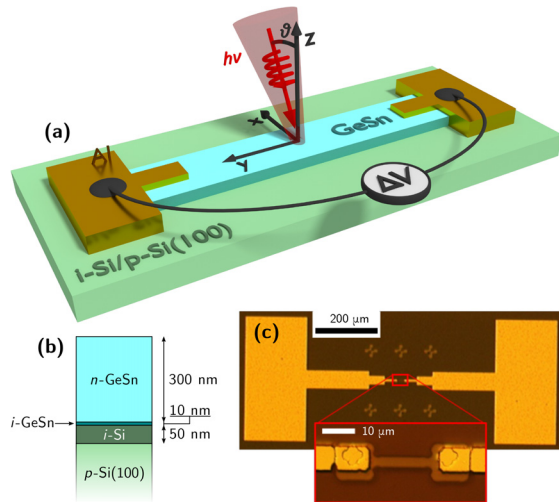
The investigated sample is a single crystalline  $n$ -doped  $\text{Ge}_{0.95}\text{Sn}_{0.05}$  stripe, grown on a  $525\text{ }\mu\text{m}$ -thick Si substrate, as sketched in Figs. 1(a) and 1(b). The GeSn is doped with antimony with concentration  $N_d = 7.4 \times 10^{17}\text{ cm}^{-3}$ , while the substrate has a boron doping  $N_a \approx 10^{16}\text{ cm}^{-3}$ . The geometrical dimensions of the stripe are  $5\text{ }\mu\text{m}$ ,  $20\text{ }\mu\text{m}$ , and  $300\text{ nm}$  along the  $x$ ,  $y$ , and  $z$  axis, respectively, within the reference frame of Fig. 1(a). An optical image of the entire investigated structure is shown in Fig. 1(c) (see the supplementary material for complete growth and fabrication details).

The geometry of the measurements is illustrated in Fig. 1(a). We exploit a supercontinuum laser<sup>37</sup> as a light source, monochromatized with a typical bandwidth of  $\approx 10\text{ meV}$  and tuned in the  $0.5\text{--}1.5\text{ eV}$  energy range. The circular-polarization of the light beam is modulated at  $50\text{ kHz}$  by a photoelastic modulator (PEM). The light beam is focused on the sample with a polar angle  $\vartheta \approx 30^\circ$ , by partially filling out-of-axis an objective with  $0.7$  numerical aperture. This results in the generation of a spin-polarization  $\mathbf{P} = P\mathbf{u}_P$  with a non-vanishing component along the  $x$ -axis since  $\mathbf{u}_P$  is antiparallel to the light wave-vector inside GeSn. The electrical ISHE signal is acquired as a voltage drop  $\Delta V_{\text{ISHE}}$  (along  $y$ ) between two Al electrodes and is demodulated with a lock-in amplifier at the PEM frequency. An off-normal illumination of the sample is fundamental since in our geometry the optically injected spin current  $\mathbf{j}_s$  diffuses along the  $z$  axis,<sup>8</sup> whereas the

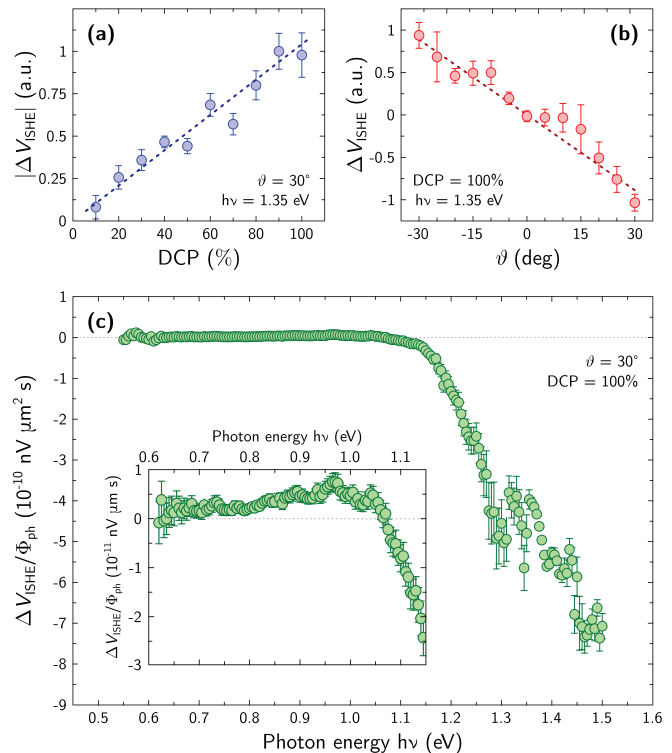
detected charge current  $\mathbf{j}_c$  flows along  $y$ . Therefore, according to Eq. (1), the projection of  $\mathbf{P}$  along  $x$  is the only detectable component of the spin polarization. To further increase the signal-to-noise ratio, the light intensity is chopped at  $1.12\text{ Hz}$  and the ISHE signal is then extracted by a second lock-in amplifier in cascade with the first one. All the measurements are performed at room temperature.

Figure 2(a) shows the dependence of the ISHE signal upon the degree of circular polarization (DCP) of the impinging light beam. This is achieved by varying the phase delay of the PEM, as detailed in the supplementary material of Ref. 13. The observed linear dependence is in agreement with calculations performed by means of multi-layer optical analysis<sup>38</sup> related to the photoinduced ISHE. In Fig. 2(b), we show the dependence of  $\Delta V_{\text{ISHE}}$  as a function of the polar angle  $\vartheta$ , defined in Fig. 1(a). The  $x$ -component of the spin polarization  $\mathbf{P}$  is opposite for opposite  $\vartheta$  values, thus yielding an opposite ISHE signal. Moreover, the ISHE signal is linear with  $\vartheta$ , as expected for small angles inside the GeSn sample (in our configuration  $\vartheta_{\text{GeSn}} < 7^\circ$ ).<sup>38</sup> The data-sets of Figs. 2(a) and 2(b) confirm the spin-related nature of the electrical signal acquired with our experimental setup.

Finally, the dependence of  $\Delta V_{\text{ISHE}}$  as a function of the incident photon energy is reported in Fig. 2(c). The experimental data are normalized to the flux of photons  $\Phi_{\text{ph}}$  transmitted into GeSn. For the sake of clarity, a zoom of the ISHE signal in the  $0.6\text{--}1.15\text{ eV}$  range is shown in the inset: in this case, it is possible to observe that the signal is



**FIG. 1.** Sample and experimental geometry. (a) A single crystalline  $\text{Ge}_{0.95}\text{Sn}_{0.05}$  stripe of dimensions  $d_x \times d_y \times d_z = 5 \times 20 \times 0.3\text{ }\mu\text{m}^3$  lies on top of a Si substrate. From two Al pads deposited onto the stripe, we measure the voltage drop  $\Delta V_{\text{ISHE}}$  due to the photoinduced ISHE. A focused circularly polarized light beam illuminates the sample at polar angle  $\vartheta$  with respect to the sample normal. (b) The molecular-beam epitaxy grown stack with doped GeSn layer on Si. (c) Optical image of the investigated sample and zoom (red inset) on the GeSn bar.



**FIG. 2.** Experimental data. [(a) and (b)] Dependence of  $\Delta V_{\text{ISHE}}$  on the degree of circular polarization (DCP) and on the polar angle  $\vartheta$ , respectively, of the impinging light beam. The dotted lines represent the linear fits of the data. (c) Photon energy dependence of  $\Delta V_{\text{ISHE}}$  normalized to the flux of photons that are transmitted into GeSn. The inset shows a zoom of the experimental data in the  $0.6\text{--}1.15\text{ eV}$  energy range.

positive for photon energies larger than 0.7 eV, and it changes sign at  $h\nu \approx 1.07$  eV. At larger photon energies, the signal rapidly increases, scaling almost linearly with  $h\nu$ . In the following, we will refer to  $\varepsilon_{SR} = 1.07$  eV as the photon energy corresponding to the sign reversal in the ISHE spectrum.

In the investigated photon energy range, optical transitions around the  $\Gamma$  point of the GeSn Brillouin zone can promote electrons from the heavy-hole (HH), light-hole (LH), and SO branches into the conduction band, as shown in Fig. 3(a), which displays the band structure of GeSn with 5% Sn concentration, calculated with a full  $\mathbf{k} \cdot \mathbf{p}$  model.<sup>19,20</sup> If the semiconductor is illuminated with a circularly polarized light beam, the spin-polarization of electrons excited from the HH branch is opposite compared to the one of electrons promoted from LH and SO bands. Moreover, the intensity of the transitions from HH, LH, and SO has a relative weight of 3, 1, and 2, respectively. This, combined with a larger joint density of states for the HH  $\rightarrow$  CB transitions, produces a net spin-polarization  $P$  at the generation time mostly given by electrons promoted from HH within the whole investigated photon energy range. This has already been demonstrated in Ge<sup>39</sup> and is further discussed in the [supplementary material](#) for GeSn. Since  $P = 50\%$  if the incident photon energy is tuned to the direct GeSn gap and monotonically decreases down to zero when the photon energy is increased,<sup>39</sup> the detected sign reversal in the ISHE spectrum cannot be ascribed to the energy dependence of the injected spin polarization.

The key ingredient to explain the experimental results of Fig. 2(c) is the dependence of the electron spin lifetime  $\tau_s$  as a function of the kinetic energy  $\varepsilon_k$ , which is reported in Fig. 3(b). Following the procedure detailed in Ref. 8,  $\tau_s$  has been calculated by accounting for the momentum scattering due to impurities and phonons (intra- and inter-valleys for all the valleys), which is related to electrons in the  $L$  and  $\Delta$  valleys. Then, the energy dependence of the spin relaxation has been evaluated by means of the Yafet–Elliott cross section.<sup>40</sup>

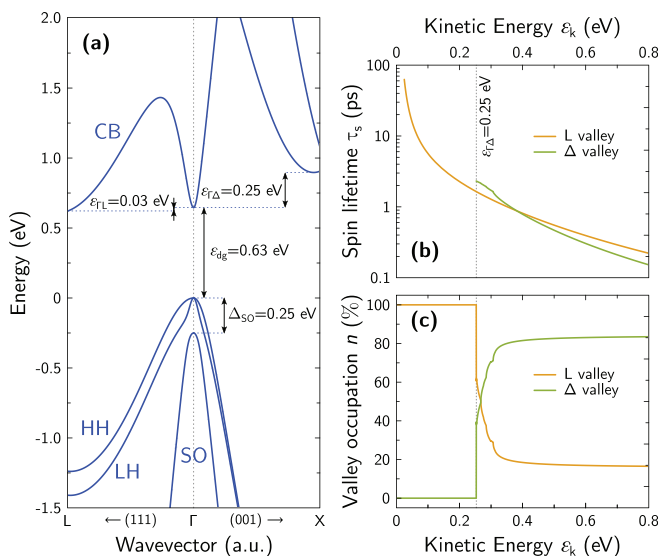


**FIG. 3.** (a) Band structure of GeSn with 5% Sn concentration, calculated within a full-band  $\mathbf{k} \cdot \mathbf{p}$  model.<sup>19,20</sup> [(b) and (c)] Kinetic energy dependence of the spin lifetime (b) and the probability of valley occupation (c), obtained from the model of Ref. 8.

Similar to the case of Ge, for  $\varepsilon_k \lesssim 0.2$  eV momentum (and spin), relaxation is mainly driven by impurities, while phonons dominate scattering at higher kinetic energies.<sup>8</sup> Due to energy conservation, electrons from the HH band are always promoted to higher energies in the CB compared to electrons coming from the SO branch. According to the results of Fig. 3(b), this means that the former experience a spin lifetime much shorter than the latter. Hence, the spin-polarized electron population coming from the HH band determines the spin polarization  $P$  at the generation time. However, such a population rapidly depolarizes and, under steady-state conditions, the spin character of the entire electron population is given mostly by spins excited from SO states. This explains the sign reversal at the onset of the optical transitions from SO and nicely fits the ISHE experimental data acquired in Ge.<sup>8</sup>

In the case of GeSn, the onset of the optical transitions from the SO band is  $h\nu = 0.88$  eV, while the sign reversal is observed at  $\varepsilon_{SR} = 1.07$  eV. Such an energy shift can be explained in a frame which accounts not only the dependence of  $\tau_s$  upon  $\varepsilon_k$ , but also the kinetic energy dependence of the valley occupation at the steady state. Figure 3(c) displays the occupation probability  $n_L$  ( $n_\Delta$ ) of the  $L$  ( $\Delta$ ) valleys as a function of  $\varepsilon_k$ , assuming  $n_\Gamma = 0$  and exploiting the model of Ref. 8. The occupation of the  $\Gamma$  valley can be set to zero due to the negligible density of states at  $\Gamma$  compared to the one at  $L$  and  $\Delta$ . From Fig. 3(c), electrons with enough kinetic energy to reach  $\Delta$  are favored to populate this valley. This is a consequence of the larger density of states at  $\Delta$  compared to the one at  $L$ . Therefore, a larger electron kinetic energy is associated with the decrease in the spin lifetime [see Fig. 3(b)] and with the increase of the population at  $\Delta$  compared to  $L$  [see Fig. 3(c)]. Notably, electrons coming from HH states start populating the  $\Delta$  valley from a photon energy  $h\nu \approx \varepsilon_{dg} + \varepsilon_{\Gamma\Delta} = 0.88$  eV [see Fig. 3(a)], which also corresponds to the onset of the transitions from the SO branch. Hence, for photon energies larger than 0.88 eV, spin-polarized electrons excited from HH diffuses at  $\Delta$ , while the electrons with opposite spin polarization promoted from the SO states are thermalized and diffuse within the  $L$  valleys.

As previously observed in GaAs,<sup>41,42</sup> the spin transport in different valleys can be associated with different spin–charge interconversion efficiencies. The reason for the shift of  $\varepsilon_{SR}$  to higher energies with respect to the onset of the optical transitions from SO states lies in a larger spin-Hall angle of electrons occupying  $\Delta$  states with respect to those lying at the  $L$  valleys. Therefore, electrons diffusing along  $\Delta$  provide a larger contribution to the ISHE signal. Thus, for  $h\nu > 0.88$  eV, although electrons coming from HH have a lower electron spin lifetime due to the larger kinetic energy, the diffusion along  $\Delta$  ensures a larger spin-to-charge conversion with respect to the electron population excited from the SO band and lying at  $L$ . In conclusion, the sign reversal of the ISHE signal is dictated by the trade-off between the energy dependence of the electron spin lifetime and the valley-dependent spin-Hall angle. It should be noted that we do not consider the hole contribution to spin transport due to the lower spin lifetime of holes compared to electrons, as we have demonstrated in Ref. 8.

We separately calculate the spatial average along the stripe thickness of the steady-state spin current densities at the  $\Delta$  and  $L$  valleys, i.e.,  $j_s^L$  and  $j_s^\Delta$ , respectively. The results are reported in Fig. 4(a), see the [supplementary material](#) for details. Due to ISHE, the spin current densities  $j_s^L$  and  $j_s^\Delta$  generate a flow of charges at  $L$  ( $j_c^L$ ) or at  $\Delta$  ( $j_c^\Delta$ ), each characterized by a spin–charge interconversion efficiency  $\gamma_L$  or  $\gamma_\Delta$ ,

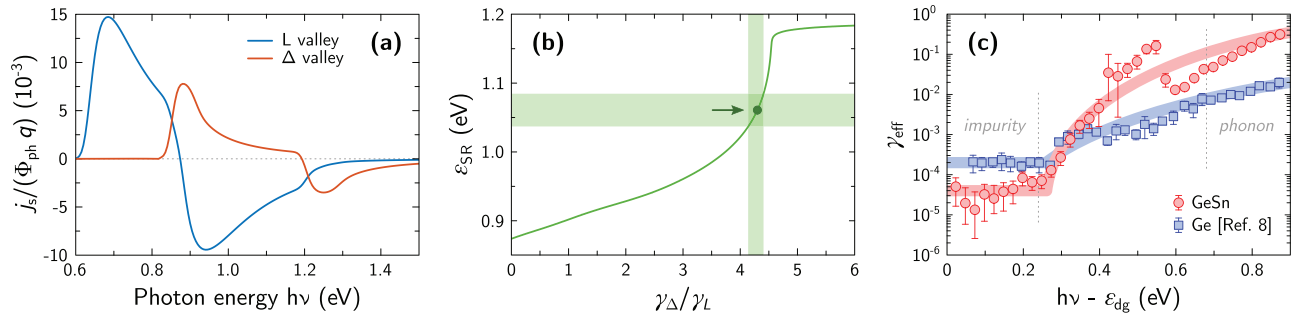


**FIG. 4.** (a) Calculation of the spin current density flowing at  $L$  and  $\Delta$  valleys as a function of the photon energy, see the [supplementary material](#) for details. Results are convoluted with a Gaussian function describing both the thermal broadening of the states ( $\approx 26$  meV) and the bandwidth of the light source ( $\approx 10$  meV). (b) Photon energy of the sign reversal  $\varepsilon_{SR}$  as a function of the relative weight of the spin-Hall angles of electrons at  $\Delta$  ( $\gamma_{\Delta}$ ) and  $L$  ( $\gamma_L$ ) valleys. The arrow corresponds to the experimental  $\varepsilon_{SR}$  value. The horizontal band accounts for the experimental error of  $\varepsilon_{SR}$ , and the vertical band is the corresponding error on  $\gamma_{\Delta} / \gamma_L$ . (c) Estimated effective spin-Hall angle (see the text) for GeSn (red circles) and Ge (blue squares, data from Ref. 8). The solid lines are guides for the eyes. Datasets are aligned to the energy of the direct gap of the materials.

respectively. Both the charge currents then contribute to the measured  $\Delta V_{ISHE}$ . Since for either  $L$  and  $\Delta$  valleys  $|\mathbf{j}_s \times \mathbf{u}_p| = j_s \sin \vartheta_{GeSn}$ , from Eq. (1), the total ISHE signal can be expressed as

$$\Delta V_{ISHE} = (\gamma_L j_s^L + \gamma_{\Delta} j_s^{\Delta}) R d \Phi_{ph} \sin \vartheta_{GeSn}, \quad (2)$$

with  $R \approx 23$  k $\Omega$  being the stripe resistance.<sup>8,41–43</sup> The sign reversal of  $\Delta V_{ISHE}$  is related to a sign reversal of the term in the parentheses. However,  $j_s^L$  and  $j_s^{\Delta}$  become negative for different photon energies [see Fig. 4(a)]: as a consequence, we can exploit the ratio  $\gamma_{\Delta} / \gamma_L$  as a free parameter to tune  $\varepsilon_{SR}$  to the experimentally detected value  $\varepsilon_{SR} = 1.07$  eV [see Fig. 2(c)]. In this case, we obtain  $\gamma_{\Delta} / \gamma_L \approx 4.3$ , meaning that the spin-orbit scattering of spin-polarized electrons at the  $\Delta$  valleys is almost 4.3 times more effective compared to the one of electrons at the  $L$  valleys. Note that in Ref. 41 the larger spin-charge interconversion at the  $L$  valleys compared to  $\Gamma$  in GaAs has been related to the larger  $p$ -like character of  $L$ . For the sake of clarity, in Fig. 4(b), we show the dependence of  $\varepsilon_{SR}$  (calculated as the photon energy by which  $\gamma_L j_s^L + \gamma_{\Delta} j_s^{\Delta} = 0$ ) as a function of the ratio between the spin-charge interconversion efficiencies  $\gamma_{\Delta} / \gamma_L$ .

A macroscopic spin-to-charge conversion parameter  $\gamma_{eff}$  can be extracted by weighting each valley-dependent spin-charge interconversion efficiency with the valley occupation,<sup>42</sup>

$$\gamma_{eff} = \gamma_L n_L + \gamma_{\Delta} n_{\Delta} \approx \gamma_L (n_L + 4.3 n_{\Delta}). \quad (3)$$

The result is reported in Fig. 4(c), where we compare  $\gamma_{eff}^{GeSn}$  with the spin-Hall angle of Ge  $\gamma_{eff}^{Ge}$ , reproduced from Ref. 8. The data are aligned to the photon energy corresponding to the direct energy gap  $\varepsilon_{dg}$ . Note that the drop of  $\gamma_{eff}^{GeSn}$  at  $h\nu - \varepsilon_{dg} \approx 0.55$  corresponds to the peak in  $j_s^{\Delta}$  at 1.25 eV [see Fig. 4(a)], which could be overestimated due to the parabolic approximation of the band structure within the employed model.

For photon energies close to  $\varepsilon_{dg}$ , where the spin-dependent scattering is mostly driven by impurities, the spin-charge interconversion is almost constant within the experimental error and  $\gamma_{eff}^{GeSn} \approx 4 \times 10^{-5}$ , while  $\gamma_{eff}^{Ge} \approx 2 \times 10^{-4}$ . In this energy range, the efficiency of spin-dependent scattering is determined by the SOC of the dopant (according to the atomic number  $Z$ ) and by the doping concentration. Despite GeSn is Sb-doped ( $Z_{sb} = 51$ ) while Ge is P-doped ( $Z_p = 15$ ),  $\gamma_{eff}^{GeSn} > \gamma_{eff}^{Ge}$  due to the large difference in the number of dopants

( $N_{sb} = 7.4 \times 10^{17}$  cm $^{-3}$ ,  $N_p = 2 \times 10^{19}$  cm $^{-3}$ ). This strongly reduces the cross section of the impurities in GeSn compared to the Ge sample. Moreover, in thin GeSn films, the large lattice mismatch between Si and GeSn leads to defect-rich material,<sup>22</sup> which contributes to further decrease the spin-Hall angle.

As observed in Ge, the spin-charge interconversion is drastically enhanced as the phonon-contribution to spin-dependent scattering increases.<sup>8</sup> Here, the spin-Hall angle of GeSn becomes larger than the one of Ge [see Fig. 4(c)]. Indeed, the phonon-mediated electron scattering mostly depends on the SOC of the lattice rather than the one of the scattering centers such as impurities, and, compared to pure Ge, the SOC of GeSn is increased by the presence of Sn. The largest spin-to-charge conversion efficiency for GeSn is  $\gamma_{eff}^{GeSn} \approx 0.3$ , at least ten times larger than the one of Ge. Notably, such a large spin-Hall angle could allow extending the lasing action already demonstrated in GeSn<sup>23</sup> to enable spin lasers where the exploitation of spin-polarized carriers could outperform the best conventional semiconductor lasers.<sup>44</sup>

We have exploited optical orientation to generate a spin-polarized electron population in the conduction band of GeSn. We have measured the inverse spin-Hall effect signal due to the spin-dependent scattering taking place in GeSn itself, and we have exploited a spin diffusion model based on the kinetic energy dependence of the spin-relaxation time to reproduce the observed ISHE spectrum. The spin-Hall angle of GeSn is more than a factor ten larger than the one of Ge, when spin-dependent scattering is mediated by phonons, due to the larger spin-orbit coupling of the GeSn lattice compared to Ge.

See the [supplementary material](#) for details about the growth and fabrication of GeSn, the optical orientation in GeSn, and the calculation of the spin current density.

## DATA AVAILABILITY

The data that support the findings of this study are available from the corresponding author upon reasonable request.

## REFERENCES

- A. V. Sadovnikov, E. N. Beginin, S. E. Sheshukova, Y. P. Sharaevskii, A. I. Stognij, N. N. Novitski, V. K. Sakharov, Y. V. Khivintsev, and S. A. Nikitov,

- “Route toward semiconductor magnonics: Light-induced spin-wave nonreciprocity in a YIG/GaAs structure,” *Phys. Rev. B* **99**, 054424 (2019).
- <sup>2</sup>D. D. Awschalom and M. E. Flatté, “Challenges for semiconductor spintronics,” *Nat. Phys.* **3**, 153–159 (2007).
- <sup>3</sup>J. Fabian, A. Matos-Abiague, C. Ertler, P. Stano, and I. Žutić, “Semiconductor spintronics,” *Acta Phys. Slovaca* **57**, 565–907 (2007).
- <sup>4</sup>K. Ando and E. Saitoh, “Observation of the inverse spin Hall effect in silicon,” *Nat. Commun.* **3**, 629 (2012).
- <sup>5</sup>F. Bottegoni, C. Zucchetti, G. Isella, E. Pinotti, M. Finazzi, and F. Ciccacci, “Modeling the photo-induced inverse spin-Hall effect in Pt/semiconductor junctions,” *J. Appl. Phys.* **124**, 033902 (2018).
- <sup>6</sup>F. Bottegoni, C. Zucchetti, F. Ciccacci, M. Finazzi, and G. Isella, “Optical generation of pure spin currents at the indirect gap of bulk Si,” *Appl. Phys. Lett.* **110**, 042403 (2017).
- <sup>7</sup>F. Bottegoni, M. Celebrano, M. Bollani, P. Biagioni, G. Isella, F. Ciccacci, and M. Finazzi, “Spin voltage generation through optical excitation of complementary spin populations,” *Nat. Mater.* **13**, 790–795 (2014).
- <sup>8</sup>C. Zucchetti, F. Bottegoni, G. Isella, M. Finazzi, F. Rortais, C. Vergnaud, J. Widiez, M. Jamet, and F. Ciccacci, “Spin-to-charge conversion for hot photo-excited electrons in germanium,” *Phys. Rev. B* **97**, 125203 (2018).
- <sup>9</sup>F. Bottegoni, C. Zucchetti, G. Isella, M. Bollani, M. Finazzi, and F. Ciccacci, “Spin-charge interconversion in heterostructures based on group-IV semiconductors,” *Riv. Nuovo Cimento* **43**, 45–96 (2020).
- <sup>10</sup>T. Guillet, C. Zucchetti, Q. Barbedienne, A. Marty, G. Isella, L. Cagnon, C. Vergnaud, H. Jaffrès, N. Reyren, J.-M. George, A. Fert, and M. Jamet, “Observation of large unidirectional Rashba magnetoresistance in Ge,” *Phys. Rev. Lett.* **124**(11), 027201 (2020).
- <sup>11</sup>C. Zucchetti, M.-T. Dau, F. Bottegoni, C. Vergnaud, T. Guillet, A. Marty, C. Beigné, S. Gambarelli, A. Picone, A. Calloni, G. Bussetti, A. Brambilla, L. Duò, F. Ciccacci, P. K. Das, J. Fujii, I. Vobornik, M. Finazzi, and M. Jamet, “Tuning spin-charge interconversion with quantum confinement in ultrathin bismuth films,” *Phys. Rev. B* **98**, 184418 (2018).
- <sup>12</sup>T. Guillet, C. Zucchetti, A. Marchionni, A. Hallal, P. Biagioni, C. Vergnaud, A. Marty, H. Okuno, A. Masseboeuf, M. Finazzi, F. Ciccacci, M. Chshiev, F. Bottegoni, and M. Jamet, “Spin orbitronics at a topological insulator-semiconductor interface,” *Phys. Rev. B* **101**, 184406 (2020).
- <sup>13</sup>C. Zucchetti, A. Ballabio, D. Chrastina, S. Cecchi, M. Finazzi, M. Virgilio, G. Isella, and F. Bottegoni, “Probing the in-plane electron spin polarization in Ge/Si<sub>0.15</sub>Ge<sub>0.85</sub> multiple quantum wells,” *Phys. Rev. B* **101**, 115408 (2020).
- <sup>14</sup>C. Zucchetti, F. Bottegoni, C. Vergnaud, F. Ciccacci, G. Isella, L. Ghirardini, M. Celebrano, F. Rortais, A. Ferrari, A. Marty, M. Finazzi, and M. Jamet, “Imaging spin diffusion in germanium at room temperature,” *Phys. Rev. B* **96**, 014403 (2017).
- <sup>15</sup>C. Zucchetti, M. Bollani, G. Isella, M. Zani, M. Finazzi, and F. Bottegoni, “Doping dependence of the electron spin diffusion length in germanium,” *APL Mater.* **7**, 101122 (2019).
- <sup>16</sup>K. Hamaya, Y. Fujita, M. Yamada, M. Kawano, S. Yamada, and K. Sawano, “Spin transport and relaxation in germanium,” *J. Phys. D: Appl. Phys.* **51**, 393001 (2018).
- <sup>17</sup>P. Li, Y. Song, and H. Dery, “Intrinsic spin lifetime of conduction electrons in germanium,” *Phys. Rev. B* **86**, 085202 (2012).
- <sup>18</sup>V. R. D’Costa, C. S. Cook, A. G. Birdwell, C. L. Littler, M. Canonico, S. Zollner, J. Kouvetakis, and J. Menéndez, “Optical critical points of thin-film Ge<sub>1-y</sub>Sn<sub>y</sub> alloys: A comparative Ge<sub>1-y</sub>Sn<sub>y</sub>/Ge<sub>1-x</sub>Si<sub>x</sub> study,” *Phys. Rev. B* **73**, 125207 (2006).
- <sup>19</sup>Z. Song, W. Fan, C. S. Tan, Q. Wang, D. Nam, D. H. Zhang, and G. Sun, “Band structure of Ge<sub>1-x</sub>Sn<sub>x</sub> alloy: A full-zone 30-band k p model,” *New J. Phys.* **21**, 073037 (2019).
- <sup>20</sup>P. Moontragoon, Z. Ikončić, and P. Harrison, “Band structure calculations of Si-Ge-Sn alloys: Achieving direct band gap materials,” *Semicond. Sci. Technol.* **22**, 742–748 (2007).
- <sup>21</sup>S. Wirths, D. Buca, and S. Mantl, “Si-Ge-Sn alloys: From growth to applications,” *Prog. Cryst. Growth Charact. Mater.* **62**, 1–39 (2016).
- <sup>22</sup>M. Bauer, C. Ritter, P. A. Crozier, J. Ren, J. Menendez, G. Wolf, and J. Kouvetakis, “Synthesis of ternary SiGeSn semiconductors on Si(100) via Sn<sub>x</sub>Ge<sub>1-x</sub> buffer layers,” *Appl. Phys. Lett.* **83**, 2163–2165 (2003).
- <sup>23</sup>S. Wirths, R. Geiger, N. Von Den Driesch, G. Mussler, T. Stoica, S. Mantl, Z. Ikončić, M. Luysberg, S. Chiussi, J. M. Hartmann, H. Sigg, J. Faist, D. Buca, and D. Grützmacher, “Lasing in direct-bandgap GeSn alloy grown on Si,” *Nat. Photonics* **9**, 88–92 (2015).
- <sup>24</sup>S. De Cesari, A. Balocchi, E. Vitiello, P. Jahandar, E. Grilli, T. Amand, X. Marie, M. Myronov, and F. Pezzoli, “Spin-coherent dynamics and carrier lifetime in strained Ge<sub>1-x</sub>Sn<sub>x</sub> semiconductors on silicon,” *Phys. Rev. B* **99**, 035202 (2019).
- <sup>25</sup>H. Dery, Y. Song, P. Li, and I. Žutić, “Silicon spin communication,” *Appl. Phys. Lett.* **99**, 082502 (2011).
- <sup>26</sup>I. Žutić, A. Matos-Abiague, B. Scharf, H. Dery, and K. Belashchenko, “Proximitized materials,” *Mater. Today* **22**, 85–107 (2019).
- <sup>27</sup>I. Žutić, J. Fabian, and S. Das Sarma, “Spintronics: Fundamentals and applications,” *Rev. Mod. Phys.* **76**, 323–410 (2004).
- <sup>28</sup>H. S. Mączko, R. Kudrawiec, and M. Gladysiewicz, “Material gain engineering in GeSn/Ge quantum wells integrated with an Si platform,” *Sci. Rep.* **6**, 34082 (2016).
- <sup>29</sup>F. Pezzoli, A. Giorgioni, D. Patchett, and M. Myronov, “Temperature-dependent photoluminescence characteristics of GeSn epitaxial layers,” *ACS Photonics* **3**, 2004–2009 (2016).
- <sup>30</sup>L. Jin, H. Zhu, D. Zhang, B. Liu, H. Meng, X. Tang, M. Li, Z. Zhong, and H. Zhang, “Spin pumping and laser modulated inverse spin Hall effect in yttrium iron garnet/germanium heterojunctions,” *Appl. Phys. Lett.* **116**, 122405 (2020).
- <sup>31</sup>G. Lampel, “Nuclear dynamic polarization by optical electronic saturation and optical pumping in semiconductors,” *Phys. Rev. Lett.* **20**, 491–493 (1968).
- <sup>32</sup>D. T. Pierce and F. Meier, “Photoemission of spin-polarized electrons from GaAs,” *Phys. Rev. B* **13**, 5484–5500 (1976).
- <sup>33</sup>F. Meier and B. P. Zakharchenya, *Optical Orientation* (Elsevier, 1984).
- <sup>34</sup>F. Bottegoni, A. Ferrari, G. Isella, M. Finazzi, and F. Ciccacci, “Enhanced orbital mixing in the valence band of strained germanium,” *Phys. Rev. B* **85**, 245312 (2012).
- <sup>35</sup>M. Dyakonov and V. Perel, “Possibility of orienting electrons spins with current,” *JETP Lett.* **13**, 467–469 (1971).
- <sup>36</sup>M. Dyakonov and V. Perel, “Current-induced spin orientation of electrons in semiconductors,” *Phys. Lett. A* **35**, 459–460 (1971).
- <sup>37</sup>SuperK Extreme EXW-12, NKT Photonics. The laser delivers nanosecond pulses at a 78 MHz repetition rate. Here, we do not exploit the temporal structure of the laser source. Indeed, our results are time-averaged since the temporal average of the time-dependent spin drift-diffusion equation equals the solution for the spin drift-diffusion equation in the steady-state, see Ref. 43. Compared to other light sources, the exploitation of a laser allows higher optical power together with high-precision control of the beam thanks to the coherency of the wavefront.
- <sup>38</sup>K. Ando, M. Morikawa, T. Trypiniotis, Y. Fujikawa, C. H. W. Barnes, and E. Saitoh, “Direct conversion of light-polarization information into electric voltage using photoinduced inverse spin-Hall effect in Pt/GaAs hybrid structure: Spin photodetector,” *J. Appl. Phys.* **107**, 113902 (2010).
- <sup>39</sup>J. Rioux and J. E. Sipe, “Optical injection and control in germanium: Thirty-band  $k \cdot p$  theory,” *Phys. Rev. B* **81**, 155215 (2010).
- <sup>40</sup>C. Guite and V. Venkataraman, “Temperature dependence of spin lifetime of conduction electrons in bulk germanium,” *Appl. Phys. Lett.* **101**, 252404 (2012).
- <sup>41</sup>N. Okamoto, H. Kurebayashi, T. Trypiniotis, I. Farrer, D. A. Ritchie, E. Saitoh, J. Sinova, J. Mašek, T. Jungwirth, and C. H. W. Barnes, “Electric control of the spin Hall effect by intervalley transitions,” *Nat. Mater.* **13**, 932–937 (2014).
- <sup>42</sup>P. Mudi, S. K. Khamari, and T. K. Sharma, “Role of hot electrons in the development of GaAs-based spin Hall devices with low power consumption,” *Phys. Status Solidi RRL* **14**, 2000097 (2020).
- <sup>43</sup>C. Zucchetti, G. Isella, F. Ciccacci, M. Finazzi, and F. Bottegoni, “Spin transport and spin-charge interconversion phenomena in Ge-based structures,” *Proc. SPIE* **11090**, 1109033 (2019).
- <sup>44</sup>M. Lindemann, G. Xu, T. Pusch, R. Michalzik, M. R. Hofmann, I. Žutić, and N. C. Gerhardt, “Ultrafast spin-lasers,” *Nature* **568**, 212 (2019).